of the film itself. However, the post-annealing in air yielded not only crystallization of the $CaTiO_3$ film but also the formation of a titanium-oxide layer in the interface between the film and the titanium substrate because of the oxidation of titanium, resulting in a change in the interface properties.

Some of the authors showed that the adhesion strength of the $CaTiO_3$ film increases with a decrease in the thickness of the interfacial TiO_2 layer [15]. By thinning the TiO_2 layer up to half its thickness, the adhesion strength estimated by the tensile test increased by approximately 40%. Likewise, Kobayashi et al. reported that, in the case of sodium titanate film, the formation of an interfacial TiO_2 layer formed by heating weakened the adhesion strength [18]. Consequently, in order to obtain a non-destructive bioactive $CaTiO_3$ layer, development of new coating process without formation of the thick oxide layer is required.

In the present study, characteristics of $CaTiO_3$ films on titanium deposited both by reactive sputtering and by pulsed laser deposition techniques were investigated. In both techniques, titanium substrates were kept at 873 K to obtain a crystallized $CaTiO_3$ film without post-annealing. Chemical states and atomic concentration of elements of deposited $CaTiO_3$ film were characterized with X-ray photoelectron spectroscopy (XPS), and crystal phase was identified with grazing incident angle X-ray diffractometry (GI-XRD). The thickness of the titanium-oxide layer formed in the interface was evaluated by depth analysis with Auger electron spectroscopy (AES).

2. Experimental procedure

2.1. Deposition of $CaTiO_3$ thin film

Commercial pure titanium (cpTi) with a purity of 99.9% (Furuuchi Chem. Co., Japan) was used as a substrate. The titanium disk (Φ 8 mm × t 1 mm) was mechanically polished with SiC paper (#1000). After polishing, the titanium disk was washed ultrasonically in acetone. The $CaTiO_3$ targets used for reactive sputtering and pulsed laser deposition techniques were prepared by the following sintering method: a commercial regent of $CaTiO_3$ with a purification of 99.9% was compacted into an appropriate dimension for the target by cold press, and the $CaTiO_3$ compact was sintered at 1523 K for 10.8 ks.

In both of the deposition processes, the cpTi substrate was kept at 873 K during the deposition, and the thickness of deposited $CaTiO_3$ films was adjusted to ca. 50 nm by controlling the deposition time. The deposition time was calculated from the deposition rate determined by a stylus-type surface profiler. The deposition rate of reactive sputtering deposition decreased with an increase of the reaction gases, whereas that of the pulsed laser deposition was constant.

For the reactive sputtering deposition, a radiofrequency (RF) magnetron sputtering system with a $CaTiO_3$ target was used [14,15]. The pressure of the deposition chamber just before the deposition (base pressure) was approximately 10^{-7} Pa. High-purity argon and oxygen gases were introduced into the chamber through a mass flow controller as working and reaction gases, respectively. The deposition was carried out in oxygen flows of 1, 3, 5, and 10 sccm. The RF power supply of the target was fixed at 200 W, and the target-to-substrate distance was 250 mm.

For the pulsed laser deposition, a third harmonic wavelength of a Q-switch pulsed Nd:YAG laser (Spectron Laser System SL805, $\lambda = 335$ nm and repetition: 10 Hz) was used for the ablation. The laser beam was introduced into a deposition vacuum chamber through a quartz window and irradiated on the $CaTiO_3$ target at a 45-degree angle to the surface. The target-to-substrate distance was 60 mm. Power density of the laser output was 2×10^4 J m^{-2}. The base pressure of the chamber was approximately 10^{-7} Pa, and the pulsed laser deposition was carried out in oxygen atmospheres at pressures of 0.13, 1.3, and 13 Pa.

2.2. Characterization of the deposited $CaTiO_3$ film

The chemical state and its composition at the film surface were analyzed with XPS. The photoelectrons were excited by Al Kα radiation (hν = 1486.6 eV) from a monochromatized X-ray source (SSX-100, Surface Science Inc., U.S.A). The spot size of the X-ray on the specimen was approximately 300×500 μm^2. The binding energy and FWHM of Au $4f_{7/2}$ were 84.0 and 1.1 eV, respectively. The atomic ratio of titanium to calcium was estimated from the integrated intensities of Ti $2p_{3/2}$ and Ca $2p_{3/2}$, where the sensitivity factors installed in the standard SSI software were used for the calculation. Crystal phase was identified by GI-XRD with a step-scanning mode at 1.3×10^{-2} deg s^{-1} and the X-ray incident angle $\alpha = 1.0°$ against the specimen surface (Rotaflex RU-200B, Rigaku, Japan). Depth profiles of the elements were determined with AES

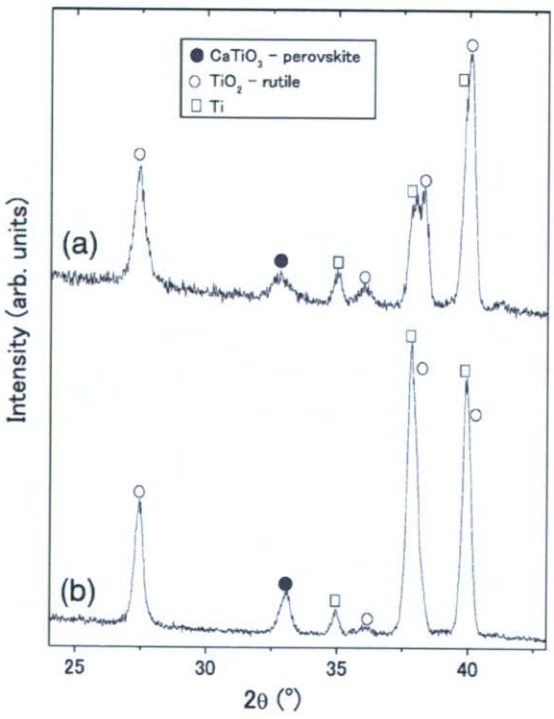

Fig. 1. GI-XRD patterns of $CaTiO_3$ thin film deposited on titanium: (a) by reactive sputtering with a 10-sccm oxygen flow, (b) by pulsed laser deposition in an oxygen atmosphere at a pressure of 1.3 Pa.

(JAMP-7100E, JEOL, Japan) with an argon-ion sputtering system. The acceleration voltage of the electron probe was 10 kV, and that of Ar ions for ion sputtering was 3.0 kV. The sputtering rate was estimated with SiO_2 film on Si substrate. The profiles were determined by monitoring differential spectra for Ti $L_3M_{23}M_{23}$, Ca $L_3M_2M_3$, and O KVV transition lines.

3. Results and discussions

3.1. Characteristics of the deposited $CaTiO_3$ thin films

Typical GI-XRD patterns of the $CaTiO_3$ deposited on the titanium are shown in Fig. 1. Since the effective depth of GI-XRD analysis at $\alpha = 1°$ is larger than the thickness of the film, the GI-XRD patterns include the peaks from the deposited film, interface layers between the film and the titanium substrate, and the titanium substrate. In the both patterns, peaks are assigned to perovskite-type $CaTiO_3$, rutile-type TiO_2, and Ti peaks. The origin of the TiO_2 is the titanium-oxide layer formed in the interface, which is revealed in the AES depth profiles shown later. It is clear that the origins of the $CaTiO_3$ and Ti peaks are the deposited film and substrate, respectively. The $CaTiO_3$ layer is crystallized by heating the substrate during the deposition. This result indicates that substrate heating at 873 K is an appropriate technique for obtaining crystallized $CaTiO_3$ film.

XPS survey spectra for the deposited films contained the peaks originating from calcium, titanium, oxygen, and carbon. The origin of carbon was surface contamination adsorbed by exposure to the atmosphere. Typical XPS spectra for Ca 2p, Ti 2p, and O 1s regions are shown in Fig. 2. Results of peak fitting analysis with Gaussian–Lorentz function are also overlapped on the spectra. XPS spectra of Ca 2p and Ti 2p consist of two peaks, corresponding to doublet by spin–orbital splitting. The binding energy of the Ti $2p_{3/2}$ peak is 458.5 eV, indicating tetravalence titanium [16,19]. The binding energy of the Ca $2p_{3/2}$ peak is 346.9 eV, which is close to those of $CaTiO_3$, calcium hydroxide ($Ca(OH)_2$), and calcium oxide (CaO). It is reported that the binding energies of CaO and $Ca(OH)_2$ are slightly higher than that of $CaTiO_3$ [19]. However, these differences in the energies are too small to judge the chemical state. The XPS spectrum for the O 1s region is deconvoluted into three peaks, originating from anhydrous oxide (O^{2-}), the hydroxide group (OH^-), and adsorbed water (H_2O).

The atomic ratios of titanium to calcium ([Ti]/[Ca]) and atomic fractions of the hydroxide group ($[OH^-]/[O^{2-}]$) in the deposited films are plotted against the amount of oxygen gases, as shown in Fig. 3. In the reactive sputtering deposition (Fig. 3(a)), the [Ti]/[Ca] ratio of 1-sccm deposited film is lower than that of stoichiometric $CaTiO_3$. The [Ti]/[Ca] ratio increases and the $[OH^-]/[O^{2-}]$ ratio decreases with an increase of oxygen flow. The [Ti]/[Ca] ratio of the 10-sccm deposited film is ca. 1, which equals

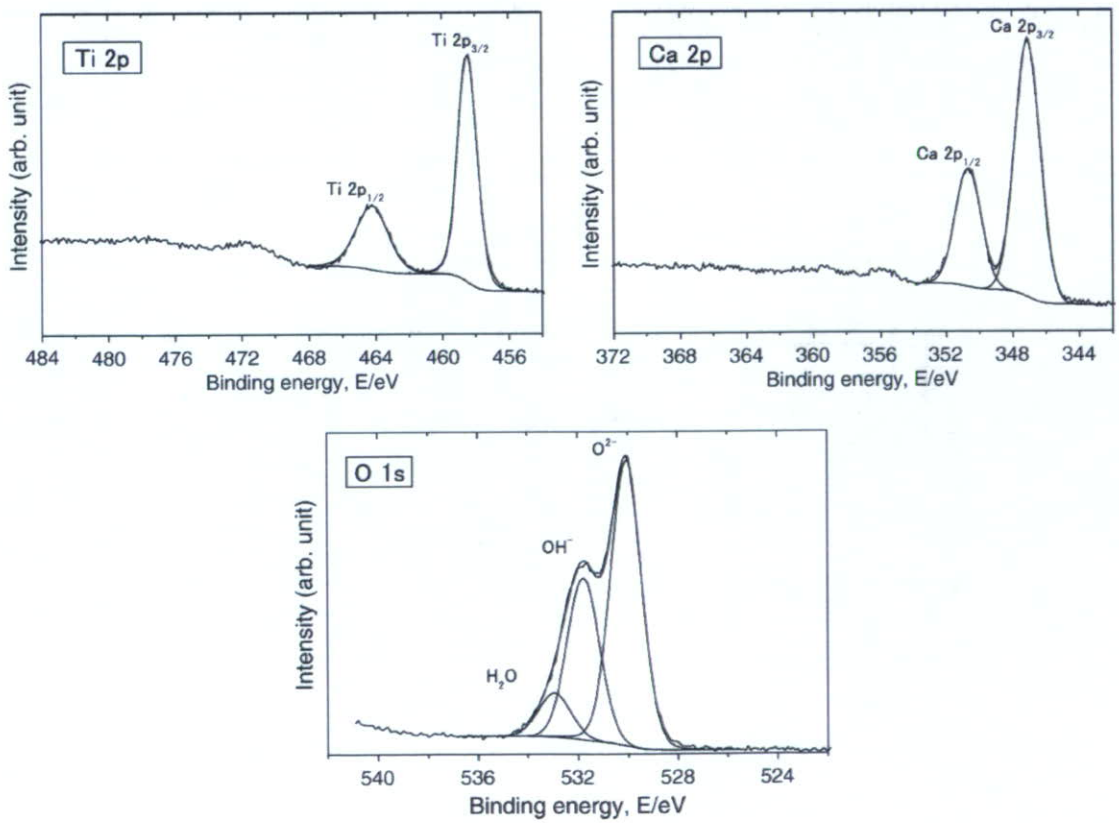

Fig. 2. XPS spectra of Ti 2p, Ca 2p, and O 1s regions for the $CaTiO_3$ film deposited by reactive sputtering with a 3-sccm oxygen flow. Results of peak fitting analysis with Gaussian–Lorentz function are also shown in the figures.

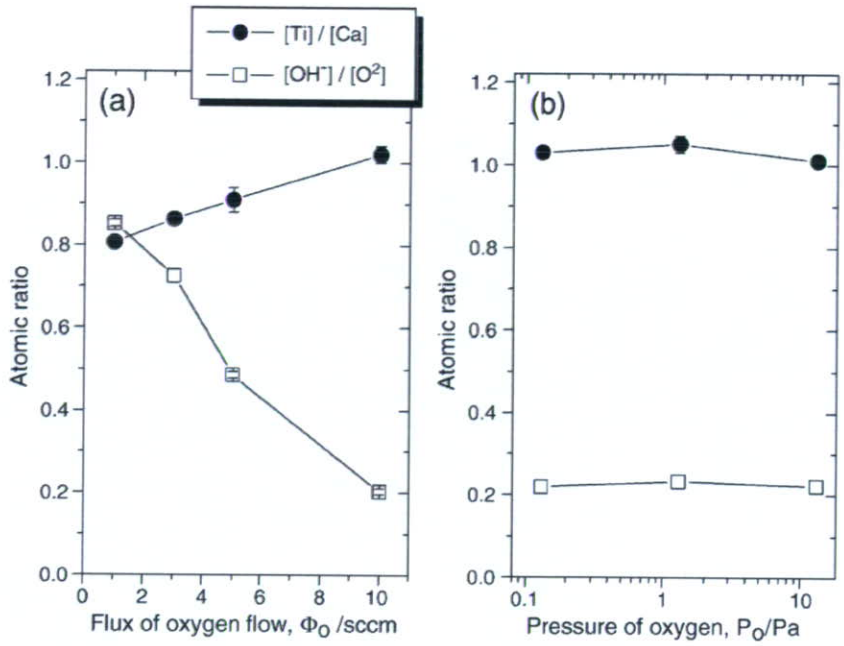

Fig. 3. Atomic ratios of titanium to calcium ([Ti]/[Ca]) and atomic fraction of hydroxide group ([OH^-]/[O^{2-}]) plotted against the amount of oxygen gases: (a) the $CaTiO_3$ films deposited by reactive sputtering, (b) the films deposited by pulsed laser deposition.

that of stoichiometiric $CaTiO_3$. On the other hand, in the pulsed laser deposition (Fig. 3(b)), the [Ti]/[Ca] ratio is almost constant at the oxygen pressure under the present experimental condition, and the value is ca. 1. Furthermore, the [OH^-]/[O^{2-}] ratio is also constant, and the value is almost in accordance with that of the film deposited by reactive sputtering with a 10-sccm oxygen flow. These results indicate that the characteristics of the $CaTiO_3$ film deposited by the reactive sputtering with a 10-sccm oxygen flow and the pulsed laser deposition with oxygen pressure in the range of 0.13 to 13 Pa are similar to each other.

3.2. Thickness of the oxide layer formed under $CaTiO_3$ thin film

Fig. 4 shows the typical depth profiles of Ca, Ti, and O for the $CaTiO_3$ film deposited on the titanium. The intensities of all signals are lower at the outermost surface due to the existence of contaminant carbon adsorbed in the air. The profiles show that the titanium-oxide layer is formed at the interface between the film and the titanium substrate.

The thicknesses of the titanium-oxide layers formed at the interface are shown in Fig. 5. Since real oxide layers may have

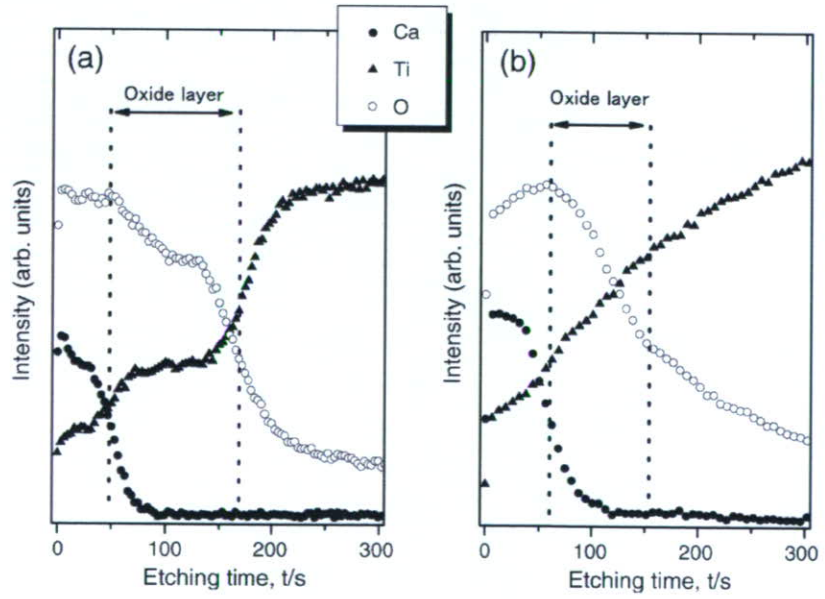

Fig. 4. Typical AES depth profiles of Ca, Ti, and O determined for the $CaTiO_3$ film deposited on titanium: (a) deposited by reactive sputtering with a 3-sccm oxygen flow, (b) deposited by pulsed laser deposition with oxygen pressure of 1.3 Pa.

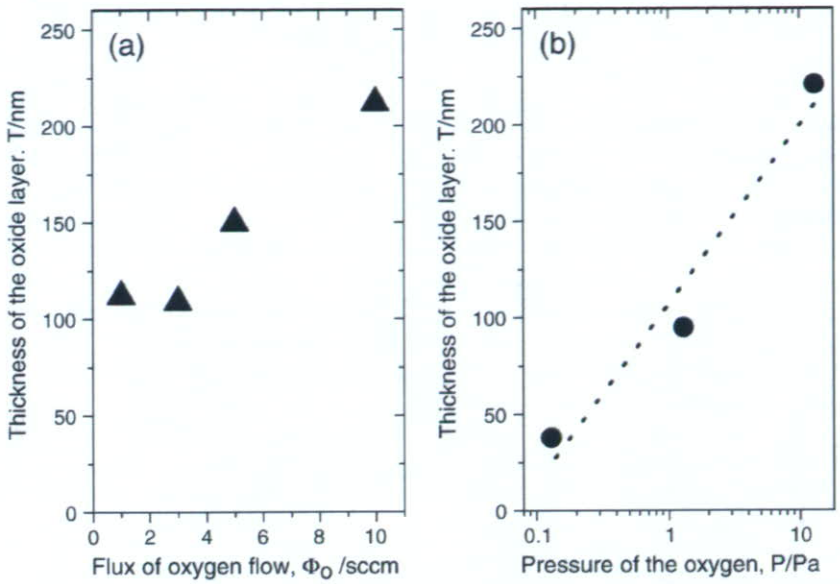

Fig. 5. Thicknesses of the titanium-oxide layer plotted against the amount of oxygen gases: (a) prepared by reactive sputtering, (b) prepared by pulsed laser deposition.

rough interface in the subnano-scale range, there is no clear boundary between the oxide layer and film or the substrate. In the present study, the titanium-oxide layer is defined as the region between the points where the intensities of Ca and O decrease to 50% in the depth profile. This definition is the same as that used in our previous study [15]. In the reactive sputtering deposition, the thickness of the oxide layer is almost constant up to a 3-sccm oxygen flow. Beyond a 3-sccm oxygen flow, the thickness increases with an increase of the oxygen flow. In order to obtain a $CaTiO_3$ film whose [Ti]/[Ca] ratio is equal to stoichiometric $CaTiO_3$, 10-sccm oxygen flow is necessary for preparation. Therefore, the formation of about a 220-nm thick titanium-oxide layer is unavoidable.

In the pulsed laser deposition, the thickness of the titanium-oxide layer is nearly proportional to the logarithm of the oxygen pressure ranging from 0.13 to 1.3 Pa. Since the stoichiometric $CaTiO_3$ film can be deposited with the oxygen pressure under the present experimental range, pulsed laser deposition makes it possible to form the stoichiometric $CaTiO_3$ thin film, the interface of which has a 40-nm oxide layer.

In comparison to the reactive sputtering and pulsed laser deposition techniques, it can be said that the pulsed laser deposition technique has an advantage in the formation of a stoichiometric $CaTiO_3$ thin film without a thick titanium-oxygen layer. This advantage is caused by the deposition rate. The deposition rate in the reactive sputtering deposition decreases with an increase of the oxygen flow [20], whereas the rate of the pulsed laser deposition is hardly changed. In the present study, the deposition rate of $CaTiO_3$ film by pulsed laser deposition was almost two times that by the reactive sputtering deposition with a 10-sccm oxygen flow.

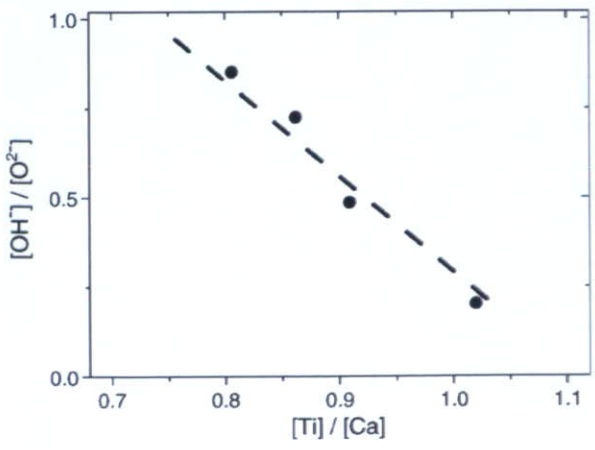

Fig. 6. Atomic fractions of hydroxide group ($[OH^-]/[O^{2-}]$) in the film deposited by reactive sputtering are plotted against the titanium-to-calcium ([Ti]/[Ca]) ratios.

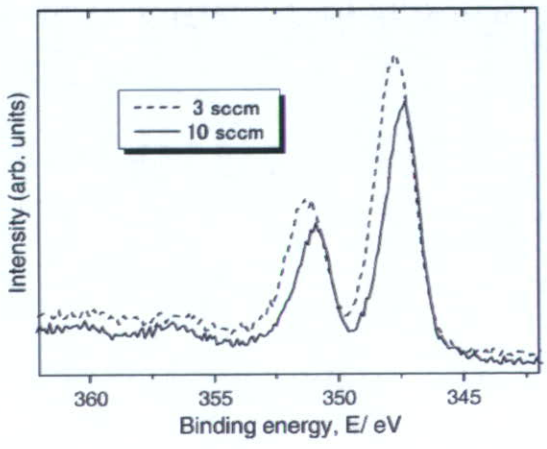

Fig. 7. Overlapping of the XPS spectra of the Ca 2p region for the film deposited by reactive sputtering with 3- and 10-sccm oxygen flows.

3.3. Relationship between the oxygen flow and film characteristics

In the reactive sputtering with oxygen flow in the range of 1 to 5 sccm, the [Ti]/[Ca] ratio of the deposited film was lower than that of stoichiometric $CaTiO_3$; in other words, calcium in the film is rich. Furthermore, in the Ca-rich films, the $[OH^-]/[O^{2-}]$ ratio is large. In Fig. 6, the $[OH^-]/[O^{2-}]$ ratios in the Ca-rich film are plotted against the [Ti]/[Ca] ratios. A good correlation between the [Ti]/[Ca] and $[OH^-]/[O^{2-}]$ ratios is observed. These results indicate that the Ca-rich film would contain not only $CaTiO_3$ but also $Ca(OH)_2$. The XPS spectra of the Ca 2p region for the film deposited with 3- and 10-sccm oxygen flows are overlapped in Fig. 7. It is clear that the peak width of the 10-sccm film is thinner than that of the 3-sccm film. Furthermore, the binding energy of Ca 2p peak for 10-sccm film is shifted to the lower energy side than that of 3-sccm film. The thinning of the Ca 2p peak and the shift of the binding energy are caused by the disappearance of $Ca(OH)_2$. These results provide direct support for $Ca(OH)_2$ formation in the Ca-rich film.

4. Conclusion

The $CaTiO_3$ thin films prepared by reactive sputtering and pulsed laser depositions are characterized by XPS, GI-XRD, and AES. The following conclusions are drawn:

1. In the reactive sputtering deposition, with an increase of oxygen flow, the titanium-to-calcium ratio of the deposited film approaches the ratio of stoichiometric $CaTiO_3$.
2. In the pulsed laser deposition, the titanium-to-calcium ratio is constantly near unity at the oxygen pressure in the range of 0.13 to 13 Pa.
3. In both deposition techniques, the crystallized $CaTiO_3$ film is obtained by heating the titanium substrate at 873 K, whereas the titanium-dioxide layer is formed at the interface between the film and the titanium substrate.
4. In both deposition techniques, the thickness of the titanium-dioxide layer increases with an increase of the amount of oxygen gases. The pulsed laser deposition has an advantage in formation of the stoichiometric $CaTiO_3$ film without formation of a thick titanium-oxide layer.
5. The film deposited by reactive sputtering with a low oxygen flow consists of calcium titanate and calcium hydroxide. The composition of calcium hydroxide decreases with an increase of the oxygen flow.

Acknowledgements

The authors gratefully acknowledge Prof. K. Asami for critically reviewing the manuscript. The authors are also grateful to Mr. Y. Murakami for supporting the AES measurement.

References

[1] K. Yamashita, E. Yonehara, X. Ding, M. Nagai, T. Umegaki, M. Matsuda, J. Biomed. Mater. Res. 43 (1998) 46.
[2] N. Yoshinari, Y. Ohtsuka, T. Derand, Biomaterials 15 (1994) 529.
[3] J.L. Ong, L.C. Lucas, Biomaterials 15 (1994) 337.
[4] K. van Dijk, H.G. Schaeken, J.G. Wolke, J.A. Jansen, Biomaterials 17 (1996) 405.
[5] Y.C. Tsui, C. Doyle, T.W. Clyne, Biomaterials 19 (1998) 2015.
[6] G. De Lange, C. De Putter, J. Oral Implantol. 19 (1993) 123.
[7] J.A. Jasen, J.P. van der Waerden, K. de Groot K, J. Biomed. Mater. Res. 25 (1991) 1535.
[8] H.W. Denissen, K. de Groot, P.C. Makkes, A. van den Hooff, P.J. Klopper, J. Biomed. Mater. Res. 14 (1980) 713.
[9] M. Jarcho, Clin. Orthop. 157 (1981) 259.
[10] K. De Groot, R. Geesink, C.P. Klein, P. Serekian, J. Biomed. Mater. Res. 21 (1987) 1375.
[11] R.G.T. Geesink, K. de Groot, C.P. Klein, J. Bone Jt. Surg. 70B (1988) 17.
[12] S.R. Radin, P. Ducheyne, J. Mater. Sci., Mater. Med. 3 (1992) 33.
[13] R.G.T. Geesink, K. de Groot, C.P. Klein, Clin. Orthop. 225 (1987) 147.
[14] K. Asami, K. Saito, N. Ohtsu, S. Nagata, T. Hanawa, Surf. Interface Anal. 35 (2003) 483.
[15] N. Ohtsu, K. Saito, K. Asami, T. Hanawa, Surf. Coat. Tech. 200 (2006) 5455.
[16] N. Ohtsu, K. Sato, K. Saito, K. Asami, T. Hanawa, J. Mater. Sci., Mater. Med. (in press).
[17] N. Ohtsu, K. Sato, A. Yanagawa, K. Saito, Y. Imai, T. Kohgo, A. Yokoyama, K. Asami, T. Hanawa, J. Biomed. Mater. Res. (in press).
[18] S. Kobayashi, T. Inoue, K. Nakai, Mater. Trans. 46 (2005) 207.
[19] T. Hanawa, H. Ukai, K. Murakami, J. Electron Spectrosc. Relat. Phenom. 63 (1993) 347.
[20] T. Narushima, K. Ueda, T. Goto, H. Masumoto, T. Katsube, H. Kawamura, C. Ouchi, Y. Iguchi, Mater. Trans. 46 (2005) 2246.

J Mater Sci: Mater Med (2007) 18:1009–1016
DOI 10.1007/s10856-006-0114-x

Calcium phosphates formation on $CaTiO_3$ coated titanium

Naofumi Ohtsu · Kenji Sato · Kesami Saito · Katsuhiko Asami · Takao Hanawa

Received: 9 May 2005 / Accepted: 27 January 2006 / Published online: 23 January 2007

Abstract In this study, performance of calcium phosphate formation of $CaTiO_3$ coating film on Ti in Hanks' balanced saline solution (HBSS) was investigated. $CaTiO_3$ thin films with a thickness of 50 nm were deposited on Ti using radiofrequency (RF) magnetron sputtering. The temperature of Ti substrate was adjusted to room temperature (RT) and 873 K. Thereafter, the specimens deposited at RT were annealed at 873 K in air for 7.2 ks. The films were characterized by grazing incident angle X-ray diffractometry (GI-XRD) and X-ray photoelectron spectroscopy (XPS). After immersion in HBSS for 60 d, on $CaTiO_3$ coated Ti, the formation of hydroxyapatite (HAP) was observed. Furthermore, HAP layer formed was thicker on the specimen on which $CaTiO_3$ film was deposited at RT and annealed than that prepared at 873 K. The major difference between both specimens was the chemical properties of the outermost surface. In summary, $CaTiO_3$ thin film deposited at RT and followed by annealing at 873 K for 7.2 ks in air enhances calcium phosphate formation ability on Ti.

Introduction

Titanium and its alloys have been widely used as biomedical and dental materials because of their excellent biocompatibility [1] and good mechanical properties [2]. However, it takes long time for these materials to bond directly to living bone. Improvement of bone-conductivity of these materials is demanded from biomedical field such as orthopedics and dentistry. In order to enhance the ability of these materials, various surface modification techniques have been attempted. Most of these techniques are physical coating processes with foreign calcium phosphate ceramic materials with high bone-conductivity, such as hydroxyapatite (HAP; $Ca_{10}(PO_4)_6(OH)_2$) and tricalcium phosphate (TCP; $Ca_3(PO_4)_2$). Ceramic coatings due to various deposition techniques, e.g. electrophoretic deposition [3], radiofrequency sputtering [4] and pulsed laser deposition [5], are investigated, and HAP coating with plasma spraying on Ti practically used for dental implants. However, various problems with HAP spray-coated Ti are pointed out by dentists. In particular, fragility of the coated HAP film itself and poor bonding strength between the film and substrate material are serious problems because they result in cracking of the coated film and at the interface during the clinical service [6]. Also, dissolution of the film during implantation is a serious problem because abrupt increase of Ca concentration in living body may induces inflammation.

Recently, bone-conductivity of Ti using implantation of Ca ions at 18 kV is accelerated [7]. It was also reported that the implanted Ca forms unequilibrium $CaTiO_3$ in the modified surface and it promotes the formation of calcium phosphates in the living body [8, 9]. Therefore, it is expected that the bone-conductivity of Ti surface will be enhanced by coating with such a $CaTiO_3$ film. One of the simplest methods to coat $CaTiO_3$ thin layer to Ti-base materials will be the sputter deposition of $CaTiO_3$. On the other hand, the

N. Ohtsu (✉) · K. Sato · K. Saito · K. Asami
Institute for Material Research, Tohoku University,
2-1-1 Katahira, Aoba-ku, Sendai 980-8577 Miyagi, Japan
e-mail: nohtsu@imr.edu

N. Ohtsu · T. Hanawa
Institute of Biomaterials and Bioengineering, Tokyo
Medical and Dental University, Tokyo 101-0062, Japan

minimum thickness of the $CaTiO_3$ film for the formation of calcium phosphates will be about the same with the depth of the modified surface by Ca-ions implantation. It is known that the modified depth by Ca^+ implantation to Ti at 18 kV is about 30 nm, which is about 1/1000 compared with that of the HAP film coated with plasma splaying. Generally, mechanical properties of thin film are improved by decreasing its thickness because of dispersion of stress. Consequently, surface modification by coating with $CaTiO_3$ thin film would be better alternative of a thick HAP coating.

In this study, performance of calcium phosphate formation on $CaTiO_3$ thin film deposited with radio-frequency (RF) magnetron sputtering was investigated by immersion in simulated body fluids (SBF). In general, materials which form calcium phosphates rapidly by immersion in SBF have a good bone-conductivity. In addition, we also discussed the $CaTiO_3$ film properties required to form calcium phosphate efficiently on the basis of the characterization of $CaTiO_3$ film.

Experimental procedure

Deposition of $CaTiO_3$ film on Ti

Commercially available pure Ti (cpTi) grade 2 (ISO 5832-2) with a disk shape (ϕ8 mm × t1 mm) was mechanically polished with SiC paper (#1500) to obtain a rough surface. $CaTiO_3$ films were deposited on cpTi substrate using RF magnetron sputtering with $CaTiO_3$ target in Ar gas flow. The background pressure of deposition chamber was about 10^{-7} Pa. The thickness of deposited films was estimated from the monitored sputtering rate of $CaTiO_3$ film and adjusted to about 50 nm. Sputtering power was fixed to 200 W. The $CaTiO_3$ thin film with low crystallinity dissolves rapidly in the SBF [10]. Therefore, we conducted two types of heat treatments to the film to increase the crystallinity and to prevent an abrupt dissolution: (1) the specimens were prepared at room temperature (RT), followed by annealing at 873 K for 7.2 ks in air (H1), and (2) the temperature of substrate was adjusted to 873 K during deposition (H2). For comparison, some specimens were prepared at RT but did not heat-treated. Specimen preparation conditions are summarized in Table 1.

Characterization of the $CaTiO_3$ films

Grazing incident angle X-ray diffractmetry (GI-XRD) was conducted with a step-scanning mode at 0.1 deg/min and a X-ray incident angle of 1 degree against the specimen surface (Rotaflex RU-200B, Rigaku, Japan).

X-ray photoelectron spectroscopy (XPS) was carried out in a pressure of about 10^{-8} Pa. Photoelectrons were excited by Al Kα radiation ($h\nu$ = 1486.6 eV) of a monochromatized X-ray source (SSX-100, Surface Science Inc, USA). In order to correct the electron-energy shift caused by charging effect, Au thin film with about 0.5-nm thickness was deposited on all specimens and all spectra were adjusted by taking the Au $4f_{7/2}$ peak position from the Au thin film as 84.0 eV. The photoionization cross-sections of the Ti $2p_{3/2}$, Ca $2p_{3/2}$ and O 1s peaks relative to that of C 1s peak used for quantification from the integrated intensities were 5.22, 3.35 and 2.93 [11], respectively.

Evaluation of calcium phosphate formation

Hanks' balanced saline solution (HBSS) as a SBF was employed to evaluate the performance of calcium phosphate formation. The ion concentrations of the HBSS and human blood plasma are compared in Table 2. The HBSS was prepared by dissolving reagent-grade $CaCl_2$, KH_2PO_4 3H2O, KCl, NaCl, $MgSO_4$ $7H_2O$, $NaHCO_3$, and Na_2HPO_4 (Nacalai Tesque, Inc) in deionized water (Millipore). Five each specimens prepared at RT, H1 and H2 were immersed in 12.2 mL of the HBSS at 310 K for 30, 45 and 60 d. For comparison, five cpTi, which was polished by SiC paper (#1500), were also immersed. Avoiding Si contamination eluted from the vessels [12], specimens were immersed in the vessels made of perfluoroalkoxy fluoroplastic (Tefron©PFA) and the vessel was completely sealed. The pH value of HBSS was adjusted to

Table 1 Specimen preparation conditions

Symbol	Sputtering conditions			Treatment after deposition
	Sputtering power	Thickness of $CaTiO_3$ film	Temperature of substrate	
RT	200 W	50 nm	Room temperature	No
H1	200 W	50 nm	Room temperature	Keep at 873 K for 7.2 ks. in air
H2	200 W	50 nm	873 K	No

Table 2 Ion concentrations of Hanks' balanced saline solution (HBSS) and human blood plasma

	Concentration (mol l^{-1})	
	HBSS	Blood plasma
Na^+	1.42×10^{-1}	1.42×10^{-1}
K^+	5.81×10^{-3}	5.00×10^{-3}
Mg^+	8.11×10^{-4}	1.50×10^{-3}
Ca^{2+}	1.26×10^{-3}	2.50×10^{-3}
Cl^-	1.45×10^{-1}	1.03×10^{-1}
HPO_4^{2-}	7.78×10^{-4}	1.00×10^{-3}
SO_4^{2-}	8.11×10^{-4}	1.50×10^{-3}
CO_3^{2-}	4.17×10^{-3}	2.7×10^{-2}

7.4 by the addition of dropwise HCl solution twice a week. After the allotted immersion periods, the specimens were retrieved from the HBSS, gently rinsed with distilled water, and dried in a convection oven at 313 K.

The formation of the calcium phosphate was examined using GI-XRD, scanning electron microscopy (SEM) and electron probe micro-analysis (EPMA; JXA-8621MX, JEOL Inc, Japan) equipped with wavelength dispersive X-ray spectrometory (WDS) and energy dispersive X-ray analysis (EDX). The acceleration voltage of SEM and EPMA was 10 kV. The thickness of the calcium phosphate layer was determined by the observation of the cross section view of specimens using SEM when calcium phosphate layer was sufficiently thick.

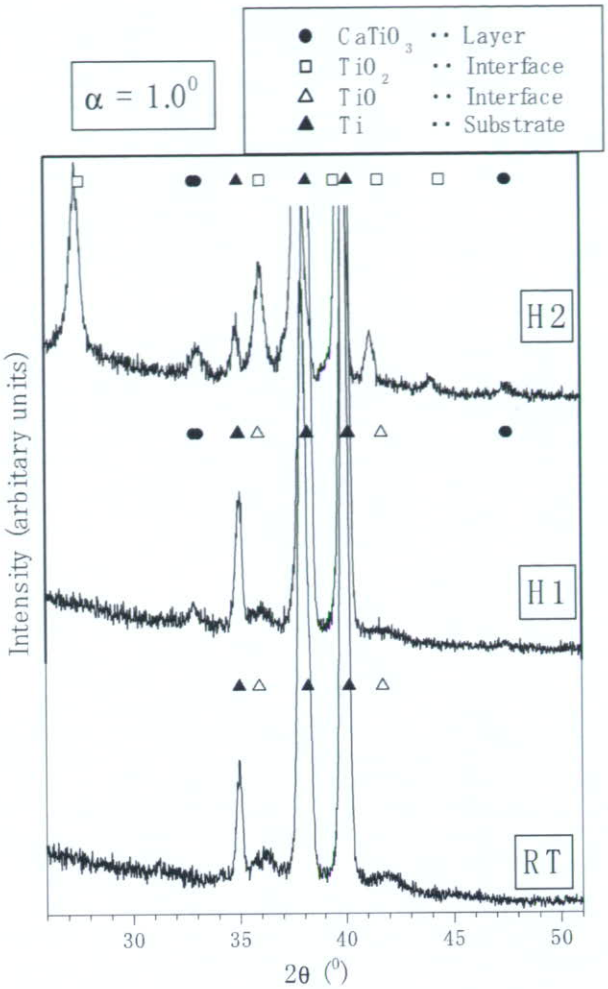

Fig. 1 GI-XRD patterns of RT, H1 and H2 specimens

Results and discussion

Characteristics of $CaTiO_3$ films before immersion

In order to utilize the surface treated cpTi and Ti-alloys in medicine and dentistry, they should be chemically stable and safe for the human body. Thus, one of the important factors for this purpose is the crystallinity of the $CaTiO_3$ film. Figure 1 shows GI-XRD patterns of the specimens before immersion. Since effective depth of GI-XRD analysis is larger than the thickness of the $CaTiO_3$ films, the GI-XRD pattern includes not only peaks from the deposited film but also those from the interface and Ti substrate. Thus, hongquiite-type TiO observed in RT and H2, and rutile type TiO_2 observed in H1 specimen were originated from the layer formed between the film and substrate. These Ti oxide layer should be formed by oxidation at the process of specimen preparation. In RT specimen, the crystallized $CaTiO_3$ was not observed. However, in both H1 and H2 specimens, perovskite-type $CaTiO_3$ was observed. These results indicate that heating at a high temperature such as 873 K is needed for the deposited $CaTiO_3$ thin film to crystallize. This crystallization temperature of $CaTiO_3$ film agrees with that of $CaTiO_3$ film prepared by sol–gel method [13].

XPS peaks of Ca 2p, Ti 2p and O 1s obtained from all specimens are shown in Fig. 2. The shape of Ca 2p peaks of RT specimen is almost symmetry, but those of H1 and H2 specimens are asymmetry and spread to higher energy side. This asymmetry is explained by the two pairs of overlapped peaks as shown in Fig. 2(a). These spectra shapes of Ca 2p and Ti 2p are similar to those of $CaTiO_3$ single-crystal [14]. The O 1s peaks of all specimens were deconvoluted into three peaks originated from anhydrous oxide (O^{2-}), hydroxyl group (OH^-) and adsorbed water (H_2O). The results are shown in Fig. 2(c). The inserted values of $\{[O^{2-}]/([OH^-] + [H_2O])\}$ to Fig. 2 are the concentration

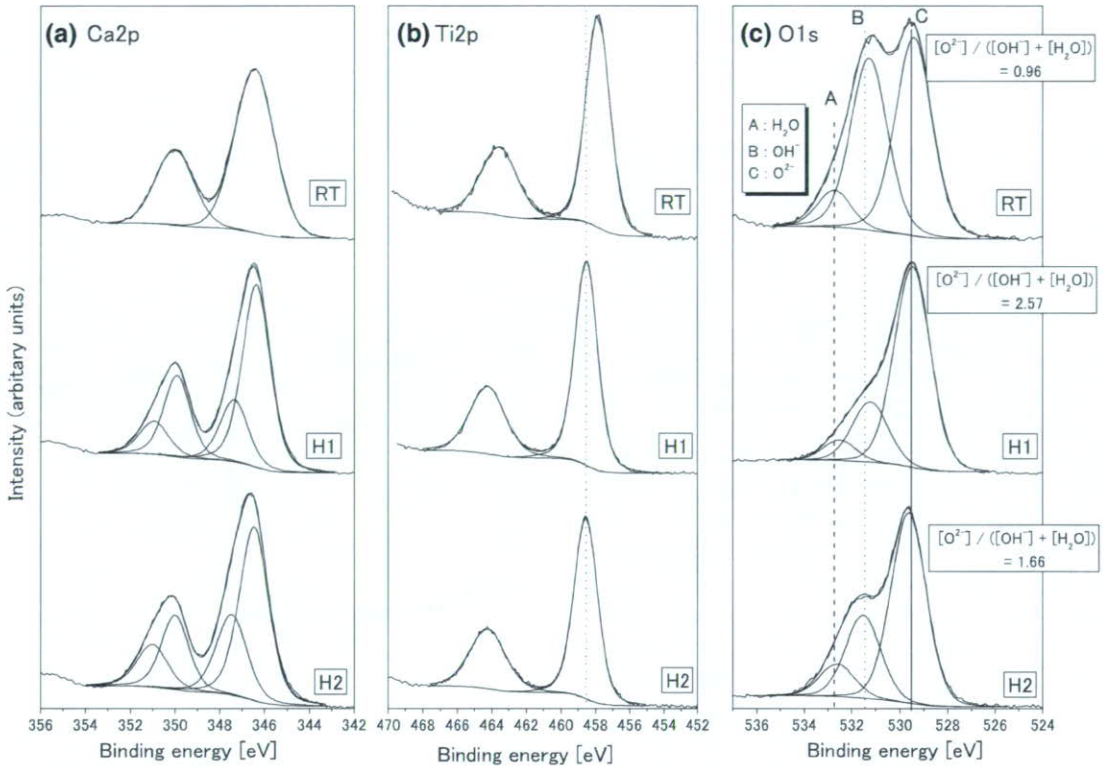

Fig. 2 XPS spectra of Ca 2p, Ti 2p and O 1s obtained from RT, H1 and H2 specimens. Binding energy values were corrected by using Au $4f_{7/2}$ = 84.0 eV. The inserted values of $\{[O^{2-}]/([OH^-] + [H_2O])\}$ are the concentration (at%) ratios calculated from the integrated intensities of O1s peaks

(at%) ratios calculated from the integrated intensities of O1s peaks. The $\{[O^{2-}]/([OH^-] + [H_2O])\}$ concentration (at%) ratios at outermost surface increases in order of RT, H2 and H1 specimens.

The binding energies of Ca $2p_{3/2}$, Ti $2p_{3/2}$, and O 1s energy region peaks are summarized in Table 3. Table 3 also contains the binding energies obtained from $CaTiO_3$, TiO_2 and CaO by a previous study [8]. The binding energies of Ca $2p_{3/2}$ level of all specimens are the almost same as those of $CaTiO_3$. The binding energies of Ti $2p_{3/2}$ level in H1 and H2 specimens are almost the same as that of $CaTiO_3$. The binding energy of Ti $2p_{3/2}$ level in RT specimen is shifted toward to the lower energy than that of $CaTiO_3$. These results indicate that the outermost surfaces in H1 and H2 specimens include the $CaTiO_3$ state. On the other hand, the outermost surface in RT specimen does not include $CaTiO_3$ state and consists of some Ca and Ti oxide states.

The results of quantitative calculation from the integrated intensities are summarized in Table 4. If the outermost surface consists of stoichiometric $CaTiO_3$, the concentration (at%) of Ti should be equal to that of Ca. The concentrations of Ti and Ca are close together in H1 specimen. On the other hand, the concentration of Ti is smaller than that of Ca in H2. These results indicate that the outermost surface in H1 specimen consists of mainly stoichiometric CaTiO, whereas that in H2 specimen include less stoichiometric $CaTiO_3$. In addition, the increase of

Table 3 Binding energies of Ca $2p_{3/2}$, Ti $2p_{3/2}$ and O1s peaks obtained from $CaTiO_3$ thin films, CaO, $CaTiO_3$, and TiO_2 using XPS. Binding energy values were corrected by using Au $4f_{7/2}$ = 84.0 eV

Specimen	Ca $2p_{3/2}$ (eV)	Ti $2p_{3/2}$ (eV)	O 1s $[OH^-]$ (eV)	O1s $[O^{2-}]$ (eV)	Reference
RT	346.8	457.9	531.5	529.5	Present work
H1	346.6	458.6	531.8	529.7	Present work
H2	346.6	458.6	531.6	529.8	Present work
$CaTiO_3$	346.6	458.4	–	–	[8]
TiO_2	–	458.8	–	–	[8]
CaO	347.2	–	–	–	[8]

Table 4 Results of quantitative calculation from the integrated intensities obtained by using XPS. [X] means concentration (at%) of the X

Specimens	$\frac{[Ca]}{([Ca]+[Ti]+[O])}$	$\frac{[Ti]}{([Ca]+[Ti]+[O])}$	$\frac{[O]}{([Ca]+[Ti]+[O])}$	$\frac{[Ti]}{[Ca]+[Ti]}$
RT	0.18	0.11	0.71	0.37
H1	0.17	0.14	0.69	0.45
H2	0.20	0.12	0.68	0.38

concentration (at%) ratio of $\{[O^{2-}]/([OH^-] + [H_2O])\}$ in H1 specimen compared with that in H2 specimen will be resulted from less hydrated surface of H1 specimen.

SEM observation of specimen surface after immersion

Since $CaTiO_3$ film in RT specimen was not crystallized and dissolved abruptly, immersion test was not performed. Figure 3 shows the SEM image of the surfaces of specimens after 30- and 60-d immersions. After immersion for 30 d (Figs. 3(a) and 3(b)), the island-like precipitates were observed on the H1 specimen. After immersion for 60 d (Figs. 3(c) and 3(d)), the surface of specimen was completely covered with precipitate layer and large size precipitates initially observed on the specimens for 30 d disappeared. The precipitate layer contained cracks in Fig. 3(d). The cracks are caused by evacuation of the water in the layer in vacuo. Figure 4 shows the EPMA-EDX spectra of precipitates observed in SEM images after 30- and 60-d immersion (Fig. 3(b) and (d)). Only the peaks from Ca and P were observed, and these precipitates were asssumed as calcium phosphates. The inserted values of [Ca]/[P] correspond to atomic ratios of the calcium phosphate determined by the EPMA-WDS. After immersion for 30 d (Fig. 4(a)), the [Ca]/[P] ratio is slightly smaller than that of HAP {[Ca]/[P] = 1.67}. After immersion for 60 d (Fig. 4(b)), the [Ca]/[P] ratio of the layer is 1.67, and this value is the same as that of HAP. In the initial stage of HAP formation, calcium phosphate with a low {[Ca]/[P]} ratio is formed. The ratio increases with time scale of days and eventually approached to that of HAP. This phenomenon was explained by a faster adsorption of phosphate ions than that of calcium ions, the adsorbed phosphate ions give negative charges at the surface and attract passively charged calcium ions [15]. Our results can be explained by essentially the same mechanism.

Figure 5 shows the SEM image of H2 specimen surface after immersion for 60 d. The surface of H2 specimen was also covered with precipitate layer. Figure 6 shows the EPMA-EDX spectrum of precipitate layer. Not only Ca and P peaks but also Ti peaks are observed in the spectrum. Ti peaks are originated from the $CaTiO_3$ film and Ti substrate because the precipitate layer is thinner than the effective depth of

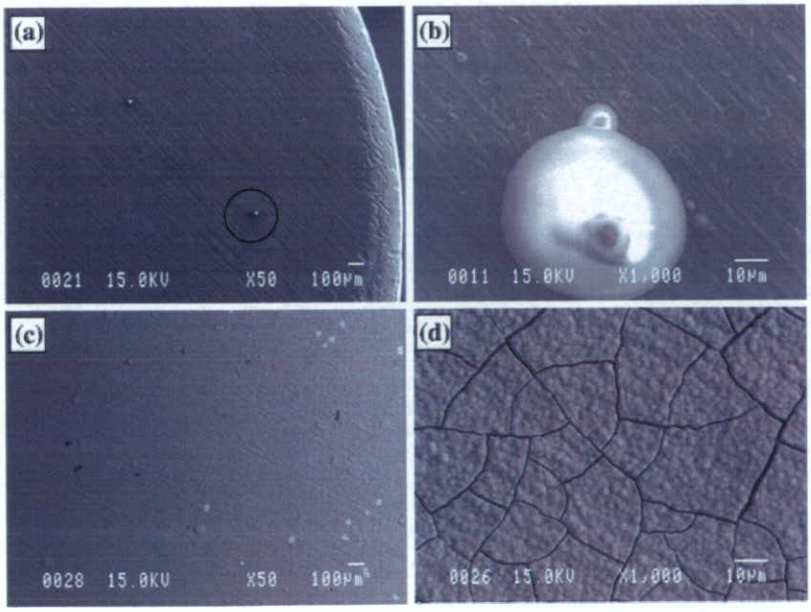

Fig. 3 SEM images of surface of H1 specimen after immersion in HBSS for 30 d (**a** and **b**) and after immersion in HBSS for 60 d (**c** and **d**)

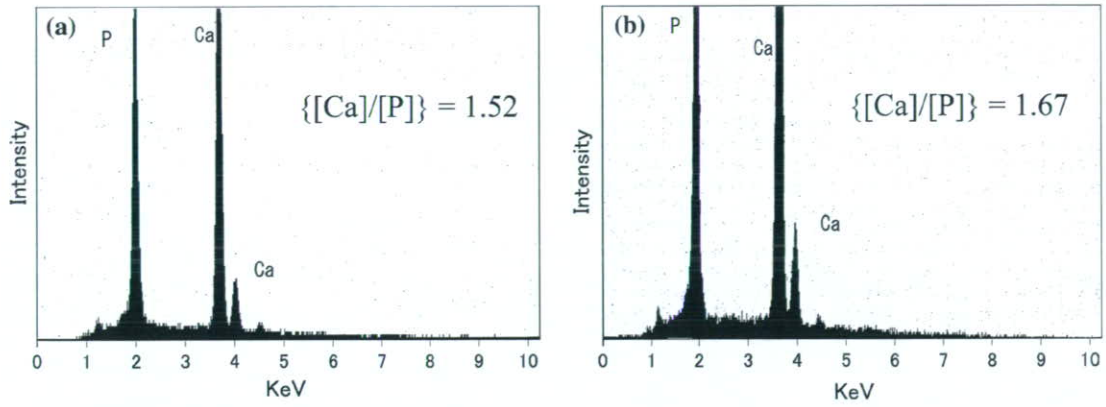

Fig. 4 EPMA-EDX spectra of precipitates of H1 specimen after immersion for 30 d (**a**) and after immersion for 60 d (**b**) in HBSS. Inserted {[Ca]/[P]} values correspond to atomic ratios of the precipitates determined by EPMA-WDS

Fig. 5 SEM images of surface of H2 specimen after immersion in HBSS for 60 d

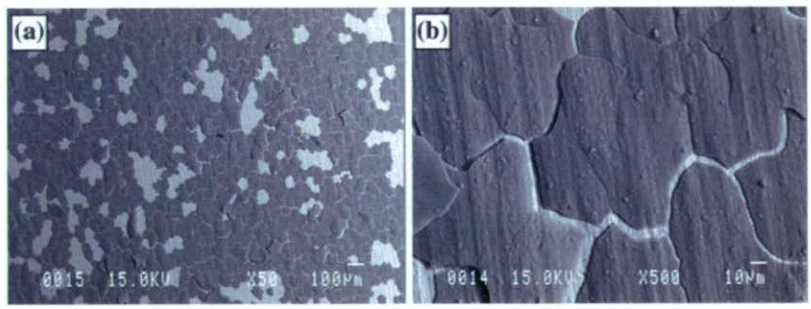

EPMA analysis. Thus, the precipitate layer is identified as calcium phosphates. The atomic ratio of {[Ca]/[P]} determined by the EPMA-WDS is also inserted in Fig. 6. The {[Ca]/[P]} ratio of the layer is slightly larger than that of HAP because Ca signal originated from the $CaTiO_3$ film is also included. The calcium phosphate layer on H2 specimen seems to be much easily peeled off from the substrate than that of H1 specimen. Furthermore, calcium phosphate was observed only on one of two H2 specimens shown in Fig. 5.

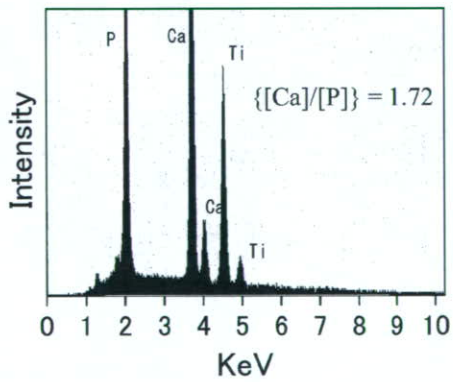

Fig. 6 EPMA-EDX spectrum of precipitates of H2 specimen after immersion for 60 d in HBSS. Inserted {[Ca]/[P]} values correspond to atomic ratios of the precipitates determined by EPMA-WDS

The results of SEM observation of all specimens are summarized in Table 5. The cpTi cannot form any calcium phosphate layer even after immersion for 60 d. Only H1 specimens can form calcium phosphate after immersion for 30, 45 and 60 d. Thus, H1 specimens showed the most stable growth of calcium phosphate layer. These results show that $CaTiO_3$ deposited 50 nm in thickness is enough to enhance the formation of calcium phosphates.

Table 5 The number of specimens formed calcium phosphate after immersion in HBSS

Specimens	30 d	45 d	60 d
cpTi	0/1	0/2	0/2
H1	1/1	2/2	2/2
H2	0/1	0/2	1/2

The number/number of specimen

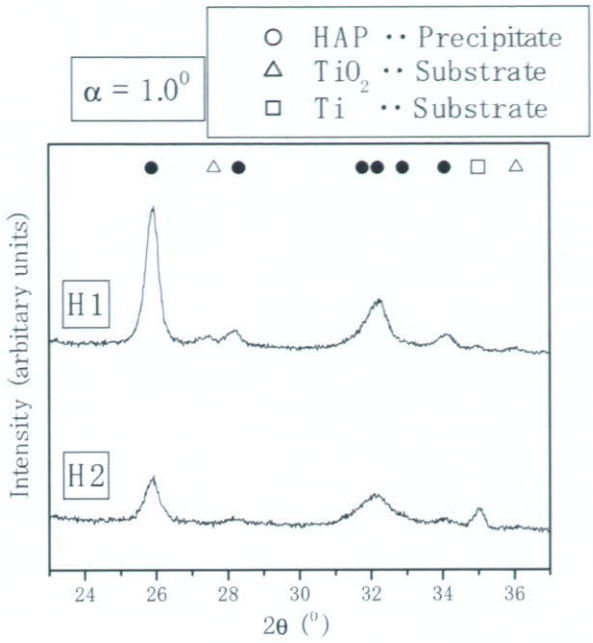

Fig. 7 GI-XRD patterns of the surface of H1 and H2 specimens after immersion in HBSS for 60 d

Figure 7 shows GI-XRD patterns of the surfaces of specimen H1 and H2 specimens after immersion for 60 d. The main peaks are assigned to reflection from HAP. Therefore, the calcium phosphate layers formed after immersion are identified as the HAP layers.

Thickness of calcium phosphate layer after immersion for 60 d

For estimating the thickness of the calcium phosphate layers formed after immersion for 60 d, the cross section of immersed specimens was observed by using SEM. Figure 8 shows the SEM images of cross section of specimens. The calcium phosphate layer on H2 specimen is very easily exfoliated from the substrate. On the other hand, it is rather strongly combined with the substrate on H1 specimen. The thicknesses of calcium phosphate layers determined from the SEM images are summarized in Table 6. The thickness of the calcium phosphate layer formed on the H1 specimen is four times as thick as that on H2 specimen. Thus, the growth rate of calcium phosphate layer on the H1 specimen is also faster than that of the H2 specimen.

Table 6 The thickness of the calcium phosphate layer formed after immersion in HBSS

Specimen	Thickness of calcium phosphate layer (μm)
H1	4.5
H2	1.2

Properties of $CaTiO_3$ film which is required to enhance calcium phosphate formation

Figures 3 and 4 show that the $CaTiO_3$ thin films of both H1 and H2 specimens can enhance the formation of calcium phosphates on Ti substrate. However, Tables 5 and 6 reveal that HAP film growth rates is large on H1 specimen. On both specimens H1 and H2, deposited $CaTiO_3$ is crystallized to perovskite-type $CaTiO_3$ and the compositions are similar. Differences are concentration of [OH] and [Ca]/[Ti] rate at the outermost surface of the deposited film.

Dissolution of Ca from the surface of materials is one of the important events for calcium phosphate formation in SBF. We consider that chemical stability at the outermost surface concern with the degradability of the film. We also attribute the high dissolution rate of Ca in H2 specimen than that in H1 specimen to the difference in the chemical stability of the outermost surface. The difference in the performance of calcium phosphate formation in H1 and H2 specimens may be caused by the difference in dissolution behavior of the outermost surface of the modified $CaTiO_3$ film deposited on Ti. However, more investigation in detail, e.g. determination of Ca amount dissolved into HBSS, is necessary to clarify this idea.

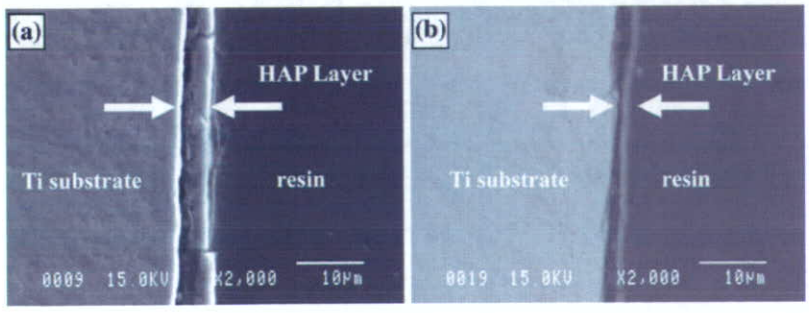

Fig. 8 SEM images of the cross section of: (**a**) H1 specimen and (**b**) H2 specimen after immersion in HBSS for 60 d

Summary

Deposition of $CaTiO_3$ at room temperature followed by annealing at 873 K in air or deposition at 873 K in vacuo could prepare the crystallized pervskite-type $CaTiO_3$ film on Ti. The outermost surfaces in both films were composed of $CaTiO_3$, whereas extent of convolution of hydroxides and other species than $CaTiO_3$ is high on the specimen deposited at 873 K and exposed to air.

After immersion in HBSS, formation of calcium phosphate was observed on $CaTiO_3$ film in both the $CaTiO_3$ film annealed in air and the $CaTiO_3$ film deposited at 873 K. The {[Ca]/[P]} ratio of the calcium phosphate formed on $CaTiO_3$ film at the initial stage is slightly smaller than that of hydroxyapatite. The ratios increased with immersion time and finally reached that of hydroxyapatite. In addition, when calcium phosphate layer was sufficiently thick, it was crystallized to hydroxyapatite. These results indicate that crystallized $CaTiO_3$ film with thickness of 50 nm can enhance the calcium phosphate formation. However, growth rate of the calcium phosphate layer is high on the specimen where the $CaTiO_3$ film was annealed in air in comparison with $CaTiO_3$ film deposited at 873 K. Therefore, in order to enhance the calcium phosphate formation efficiently, $CaTiO_3$ film should be modified by annealing in air rather than deposition on heated substrate in vacuo.

Acknowledgment The authors thank Mr. Yoshihiro Murakami for operating the EPMA.

References

1. A. YAMAMOTO, R. HONMA and M. SUMITA, *J. Biomed. Mater. Res.* **39** (1998) 331
2. M. PAPAKYRIACOU, H. MAYER, C. PYPEN, H. PLENK Jr and S. STANZ-TSCHEGG, *Int. J. Fatigue* **22** (2000) 873
3. K. YaMashita, E. YONEHARA, X. DING, M. NAGAI, T. UMEGAKI and M. MATSUDA, *Biomed. Mater. Res.* **43** (1998) 46
4. K. van DIJK, H. G. SCHAEKEN, J. G. G. WOLKE and J. A. JANSE, *Biomaterials* **17** (1996) 405
5. C. K. WANG, J. H. CHEN LIN, C. P. JU, H. C. ONG and R. P. H. CHANG, *Biomaterials* **18** (1997) 1331
6. K. A. KHOR, Y. W. GU, C. H. QUEK and P. CHEANG, *Surf. Coat. Tech.* **168** (2003) 195
7. T. HANAWA, Y. KAMIURA, S. YAMAMOTO, T. KOHGO, A. AMEMIYA, H. UKAI, K. MURAKAMI and K. ASAOKA, *J. Biomed. Mater. Res.* **36** (1997) 131
8. T. HANAWA, H. UKAI and K. MURAKAMI, *J. Electron Specctrosc. Relat. Phenom.* **63** (1993) 347
9. D. KRUPA, J. BASZKIEWICZ, J. A KOZUBOWSKI, A. BARCZ, J. W. SOBCZAK, A. BILINSKI, M. LEWANDOWSKA-SZUMIEL and B. RAJCHEL, *Biomaterials* **22** (2001) 2139
10. N. OHTSU, K. SATO, K. SAITO, T. HANAWA and K. ASAMI, *Mater. Trans.* **45** (2004) 1778
11. J. H. SCOFIELD, *J. Electron Spectrosc. Relat. Phenom.* **8** (1973) 129
12. N. OHTSU, T. ASHINO and K. ASAMI, *Mater. Trans.* **45** (2004) 550
13. S. KACIULIS, G. MATTOGNO, A. NAPOLI, E. BEMPORAD, F. FERRARI, A. MONTENERO and G. GNAPPI, *J. Electron Spectrosc.* **95** (1998) 61
14. P. A. W. van der HEIDE, *Surf. Sci.* **490** (2001) L619
15. M. UCHIDA, H. M. KIM, F. MIYAJI, T. NAKAMURA and T. KOKUBO, *J. Am. Ceram. Soc.* **84** (2001) 2041

J Mater Sci: Mater Med (2007) 18:797–806
DOI 10.1007/s10856-006-0004-2

Calcium phosphate formation on titanium by low-voltage electrolytic treatments

Y. Tanaka · E. Kobayashi · S. Hiromoto · K. Asami · H. Imai · T. Hanawa

Received: 22 July 2005 / Accepted: 5 December 2005 / Published online: 2 December 2006

Abstract Electrochemical treatments are expected to be effective for the coating of calcium phosphate ceramics to a titanium substrate. In the present study, two types of chronoamperometry with a step potential and a cyclic wave potential at low voltage (up to 2.0 V) and low current density were performed in Hanks' solution to modify the surface characteristics of titanium. Titanium oxide film formed by self-passivation, that formed as reconstructed film during electrochemical treatments, and a calcium phosphate layer precipitated through treatments were characterised by X-ray photoelectron spectroscopy. The thickness and compositions of the surface films and layers were quantified from the XPS results. Calcium phosphate formation during immersion in Hanks' solution for 1.0 Ms was evaluated by scanning electron microscopy with energy-dispersive X-ray spectrometry. The results confirmed that the electrolytic treatments in this study were effective to accelerate calcium phosphate formation on titanium in Hanks' solution in spite of their lower voltage than conventional methods. The results also suggested that the hydroxyl group in the surface oxide film might contribute to the formation of calcium phosphate. This technique is a promising process for the treatment of thin titanium materials.

Y. Tanaka · E. Kobayashi (✉) · T. Hanawa
Institute of Biomaterials and Bioengineering, Tokyo Medical and Dental University, Tokyo 101-0062, Japan
e-mail: equo.met@tmd.ac.jp

Y. Tanaka · H. Imai
Department of Materials Science and Engineering, Shibaura Institute of Technology, Tokyo 108-8548, Japan

S. Hiromoto
Biomaterials Center, National Institute for Materials Science, Tsukuba 305-0044, Japan

K. Asami
Institute for Materials Research, Tohoku University, Sendai 980-8577, Japan

1 Introduction

Titanium is known to have satisfactory biocompatibility among metallic materials. Several kinds of biomedical alloys were designed till today [1–5]. To develop bone conductivity on titanium, a biomimetic ceramic coating is necessary. The mechanical properties are the result of the characteristics of the bulk structures and that biocompatibility, including bone conductivity, is the result of the surface chemical and/or physical characteristics. Applying a ceramic coating on metals is a promising method to obtain both benefits in one process. Thus, several bioceramic coating techniques, such as bioglass, AW-glass ceramics, and hydroxyapatite ($Ca_{10}(PO_4)_6(OH)_2$), have been developed [6–8].

Plasma spray coating is a well-established ceramic coating technique, and artificial hip joints made of a Ti–6Al–4V alloy coated with hydroxyapatite have been on the market for more than a decade with successful results [9]. The plasma spray coating, however, cannot be applied in sufficient amounts on complex surfaces, such as screws and porous materials. Remaining concerns are the apatite transformation that occurs during remelting at high temperatures and the flaking off of the coated layer [10]. Some other techniques to modify the surface characteristics have been reported.

Ion plating [11] and Ca ion implantation [12, 13] are effective methods, but they require the use of large facilities.

On the other hand, electrochemical treatments are commonly used to form an apatite coating on a titanium substrate. Ban and his colleagues reported on the morphology control of an apatite coating on a titanium substrate using electrolysis techniques at higher temperatures with varied currents [14, 15]. Zhu et al. succeeded in producing a Ca- and P-enriched titanium oxide film on a titanium substrate electrochemically with 70 A m^{-2} and 350 V [16]. These processes were also useful to coat a substrate with a complex surface design. Kuroda et al. used a solution containing calcium phosphate ions and hydrogen peroxide at 150 °C to coat hydroxyl apatite with different surface morphologies on a titanium substrate [17]. You et al. recently reported making a hydroxyapatite coating on dental implants with an electrophoretic technique with 20 V [18]. By these electrochemical treatments, carbonate-containing apatite with desirable morphologies, such as a plane, needles, and particles, could be precipitated on titanium. However, the processes reported above require large current, voltage, and/or higher temperatures. By applying a very large current in excess of the passive current density, the passive film on the alloys may be damaged, and active general corrosion might occur. Porous materials and thin textures will be required for future medical technologies, such as microsurgery and tissue engineering. Treatments providing biocompatibility to those materials with complex surfaces and structures will be required. A thin texture woven with thin titanium fibres is considered to be preferable as a scaffold in tissue engineering. When large current and voltage are applied, the already thin texture easily becomes thinner or dissolves by general corrosion. To avoid these outcomes, an electrolytic treatment with lower voltage is among the better solutions.

In the present study, to enhance the calcium phosphate precipitation, electrolytic treatments applying a step potential (SP) or a cyclic potential (CP) at low voltage were carried out using an artificial biofluid to modify the surface characteristics. According to previous reports, several artificial biofluids have been used for electrochemical treatments [19]. Hanks' solution was employed in this study.

An advantageous feature of this method is not to aim to maintain calcium phosphate layer with appropriate thickness on the alloy during the treatment. It is always possible that coated layers formed before implantation will flake off in clinical usage. At a lower voltage, however, this treatment provides small nuclei of precipitation distributed on the alloy surface that act as sites of natural calcium phosphate precipitation in a living body; in other words, the specks serve as sites for new bone growth. This means that the bonding of implants and bone is guaranteed by the nature of the interface between the implant surface and self-grown bone rather than by that between the implant surface and calcium phosphate coating layer formed as a result of the electrolytic treatments.

The immersion test in Hanks' solution was carried out to simulate bone formation in a living body. To evaluate calcium phosphate formation, X-ray photoelectron spectroscopy (XPS) and scanning electron microscopy (SEM) were conducted. XPS is known as a useful method to evaluate very small amounts of precipitation that are often lower than the detection limitations of SEM and energy-dispersive X-ray spectrometry (EDS). Finally, to develop a biocompatible titanium texture as a model scaffold of tissue engineering, electrolytic treatments were applied on a flatly woven titanium texture. Calcium phosphate formation on the titanium texture was also observed using SEM.

2 Experimental

2.1 Specimens and electrolytic treatments

Commercially pure titanium disks with 8 mm and 14 mm in diameter and 2.2 mm in thickness (purity 99.5 mass%) were used in the present study. Specimens were mechanically polished with SiC papers in de-ionised water and mirror-finished with diamond paste. After being washed ultrasonically in acetone, they were dried with a nitrogen gas flow.

Two kinds of electrolytic treatments using SP and CP with low voltage were developed in the present study. Hanks' solution (pH 7.4), which simulates the inorganic composition of extracellular fluid, was employed as an electrolyte for surface modification. Schematics of the treatment procedures (applied voltage) are shown in Fig. 1.

As shown in Fig. 1(a), SP was applied in one treatment. It was a typical chronoamperometry that measured the current density change while the potential increased step-like from the rest potential, E_0, to 1.0 or 2.0 V, which was a lower voltage than that in conventional methods and still in the passive state. This treatment was performed in two different durations, 1 ks and 10 ks. A potentiostat (HZ-3000, Hokuto Denko) was used to control the potential for the SP treatment. A saturated calomel electrode (SCE) was used as a reference electrode, and platinum was used as

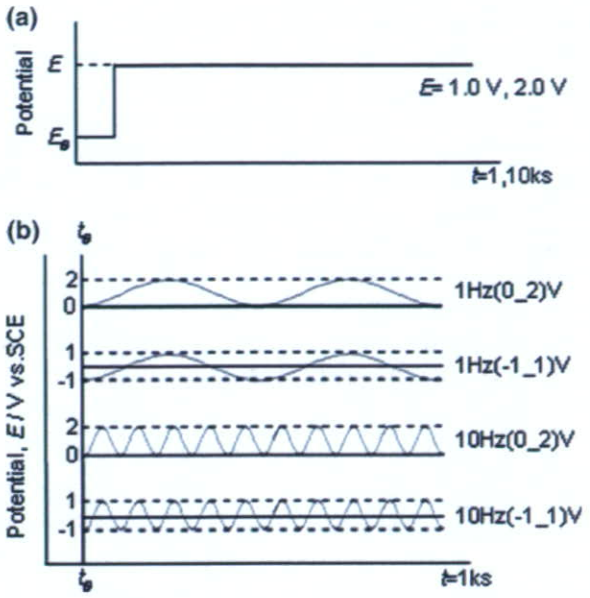

Fig. 1 Schematics of the treatment procedures showing the potential wave forms of the SP treatment (**a**) and the CP treatment (**b**)

a counter electrode. A titanium disk specimen in a Teflon holder, which was insulated from the electrolyte except for an opening window for testing, was used as a working electrode. A schematic of the working electrode is shown in Fig. 2.

In another treatment, CP with a trigonometric wave form was applied with 1 Hz or 10 Hz in frequency instead of SP, as shown in Fig. 1(b). Two different voltage waves with the same amplitude from 0 V to 2.0 V and from –1.0 V to 1.0 V were applied. For this

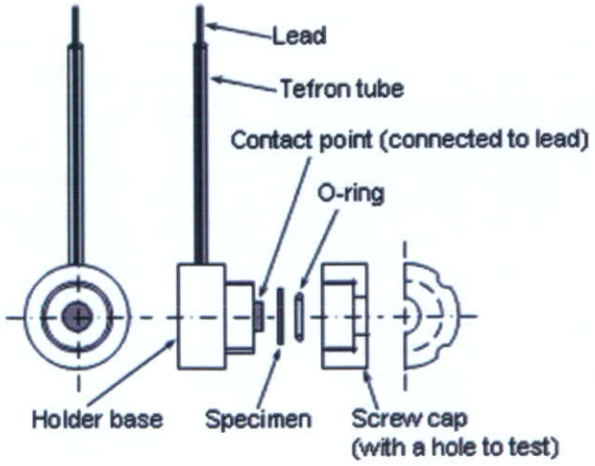

Fig. 2 Schematics of the working electrode including the specimen (titanium disk) and Teflon holder used for the SP and CP treatments. The screw cap has an opening for the test

CP treatment, a function generator (WF1946A, NF Corporation), a data acquisition system (Daq Book, Toyo Corporation), a potentiostat (HZ150G, Hokuto Denko), and data acquisition software (DASY Lab32, ADTEK System Science) to maintain the cyclic wave form were used instead of HZ–3000 in the SP treatment.

For both treatments, a test cell filled up with Hanks' solution was put in an isothermal water bath to keep the electrolyte at 310 K. The electrolyte was deaerated by high-purity nitrogen gas bubbling for 1.8 ks prior to the test.

2.2 Performance of calcium phosphate formation by immersion in Hanks' solution

To evaluate calcium phosphate formation on the surface-modified specimens, immersion in Hanks' solution was carried out after the electrolytic treatments. The specimens were immersed in Hanks' solution (42 ml) at 310 K for 1.0 Ms using sealed Teflon vessels.

2.3 XPS analysis

XPS was carried out using an X-ray photoelectron spectrometer (SSX100, SSI) in order to characterise the specimens' surface of specimens, that of after the electrolytic treatment, and that of after the electrolytic treatment and immersion in Hanks' solution. The X-ray source was monochromatised AlK_α (1486.61 eV) accelerated with 10 kV. The photoelectrons were detected through 20 eV in FAT pass energy, with a 35° take off angle.

The binding energy on the XPS spectra was corrected according to a peak binding energy of C 1s (hydrocarbon C–C and C–H) electrons at 285.0 eV due to the surface-contaminated layer [20]. The quantification of the composition and the thickness measurement of the surface films and layers were conducted with the inductive calculation method presented by Asami et al. [21], assuming stacking layers of a titanium oxide film (inner layer), a calcium phosphate layer (intermediate layer), and carbon contaminants (outer layer) on a titanium substrate.

2.4 SEM/EDS analysis

To evaluate the characteristics of calcium phosphate after immersion in Hanks' solution, SEM/EDS analysis was conducted with secondary electron images of a scanning electron microscope (JSM-5400, JEOL) at 15 kV of accelerating voltages and energy-dispersive

X-ray spectrometry (EDS) at 10 kV of accelerating voltage with 0.8 A of current density.

2.5 Electrolytic treatments on the titanium texture

In order to develop a biocompatible titanium texture, CP treatments were applied on a flatly woven titanium texture (1.0 mm in texture width, woven with eight titanium wires with a wire diameter of 0.1 mm) provided by Dr. K. Murakami of Ishikawajima-Harima Heavy Industries. Calcium phosphate formation through immersion in Hanks' solution on the titanium woven texture was observed using SEM.

3 Results

3.1 SP treatment

3.1.1 Current density response curves

The current density response curves of the SP treatments at 1.0 V for 1 ks and 10 ks are shown in Fig. 3. An inserted graph shows a close-up view of the curves within tens of seconds after the SP. The curve of the 1 ks treatment precisely overlapped with that of the 10 ks treatment even in this enlarged figure. The SP treatments at 2.0 V also showed almost identical curves. When the potential was changed from the rest potential, E_0, to a step potential (1.0 V or 2.0 V), the peak current density, I_0, appeared as the maximum value followed by steep decreasing to a very small passive current density with an asymptotic curvature. The total electric charge, Q, was calculated as a time-transient curve of the current density. For both treatment times (1 ks and 10 ks), no difference between Q and I_0 was seen because the current density had decreased asymptotically and was close to zero (in fact, it reached zero within the current resolution of the measurement system in the present study) before 1 ks. The values of I_0 and Q for each test condition are indicated in Table 1.

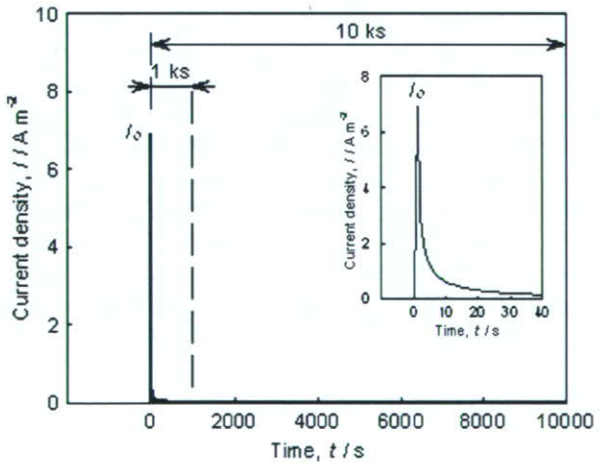

Fig. 3 Current density response curves of the SP treatments at 1.0 V for 1 ks and 10 ks showing the peak current density, I_0, and the steep decrease of the current density. An inserted graph shows a close-up view of the curves within tens of seconds after the SP

After these treatments, no sign of corrosion, including pitting and general corrosion, was observed.

3.1.2 XPS analysis

The surfaces of SP-treated specimens exhibited a slightly golden lustre. The specimen treated at 2.0 V for 10 ks had the darkest shade of golden lustre among them. This suggested the presence of some reaction product on the film that contained yellowish ions and/or interfered with the colouring on the specimens' surface. The results of a wide range of XPS spectra are shown in Fig. 4. In the spectrum of each specimen, peaks from C, O, Ti, P, Ca, and/or N were detected.

The compositions of surface films of specimens with/without SP treatment are shown in Table 2. No Ti was detected form the specimen treated at 2 V for 10 ks, while P and Ca were detected in each specimen. This suggests that a very thick phosphate layer was formed on the titanium oxide film on the surface of the specimen treated at 2.0 V for 10 ks.

Figure 5 shows the XPS analysis of the Ti 2p electron energy region on the surfaces of all specimens. The XPS spectra were decomposed into four doublets (Ti^0, Ti^{2+}, Ti^{3+}, and Ti^{4+}) with the valence according to the binding energy reported by Asami et al. [22]. All of the specimens, other than those treated at 2.0 V for 10 ks, showed Ti $2p_{3/2}$ (higher binding energy) and Ti $2p_{1/2}$ (lower) peaks of Ti^{4+}. In addition, only the untreated specimen showed a clear spectrum peak of Ti^0, which corresponds to the metallic state. A fraction of Ti^{4+} among all Ti cations, Ti^{2+}, Ti^{3+}, and Ti^{4+}, is shown in Table 3 together with the surface film

Table 1 Results of the SP treatment for the peak current density, I_0, and the total electric charge, Q, which was calculated as a time-transient curve of the current density

	Step potential	
	1 V	2 V
I_0 (A m^{-2})	6.5	6.5
Q (C m^{-2})	3.5×10^{1}	3.7×10^{1}

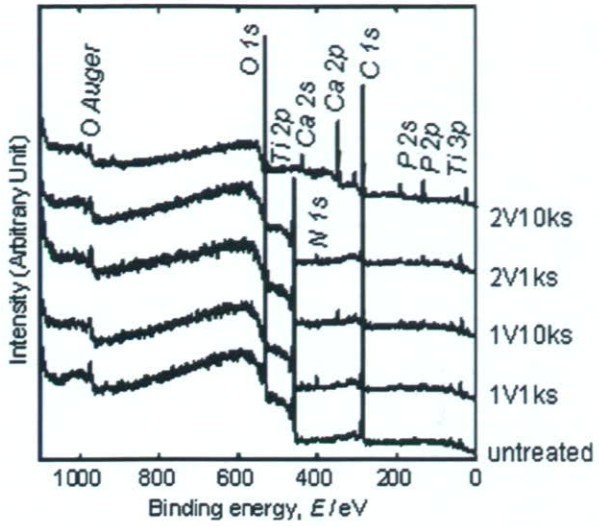

Fig. 4 Results of wide-range XPS spectra of SP-treated specimens in comparison with an untreated specimen showing C, O, Ti, P, Ca, and/or N peaks

Table 2 Compositions of the surface films of the specimens after SP treatment calculated from XPS data

	Ti	O	P	Ca
1 V–1 ks	17.19	80.79	1.63	0.38
1 V–10 ks	58.09	23.33	9.41	9.17
2 V–1 ks	18.47	79.15	2.14	0.24
2 V–10 ks	0	83.23	6.10	10.67
				(mol %)

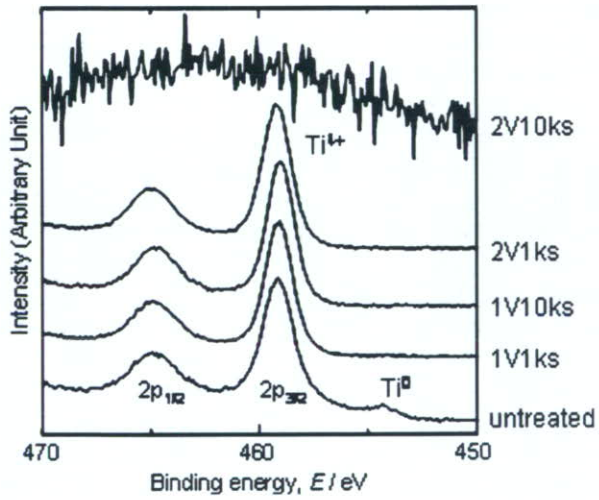

Fig. 5 Ti 2p electron energy region XPS spectra of SP-treated specimens showing Ti $2p_{3/2}$ and Ti $2p_{1/2}$ peaks of Ti^{4+}. Only the untreated specimen's spectrum showed a Ti^0 peak

thickness calculated from the XPS data. As compared to the specimen without treatment, all of the SP-treated specimens exhibited around 67% thicker surface films and an approximately 12% higher Ti^{4+} fraction. However, no significant difference in the thickness and the Ti^{4+} fraction was seen among specimens treated at 1.0 V for 1 ks, 1.0 V for 10 ks, and 2.0 V for 1 ks. The results for the specimen treated at 2.0 V for 10 ks in Tables 2 and 3 reveal that a very thick phosphate layer was formed above the titanium oxide film, which prevented the detection of any titanium cation peaks, as shown in Fig. 5.

Spectra of P 2p and Ca 2p were obtained as a set of peaks. The binding energy of P 2p electrons was 133.3–133.5 eV, while that of Ca 2p3/2 electrons was 347.3–347.6 eV in a previous study [23, 24]. According to these data, the former spectrum overlapped in the vicinity of two peaks coming from PO_4^{3-} and HPO_4^{2-}, and the latter, in the vicinity of those coming from Ca^{2+}, proving the calcium phosphate formation. The spectra of O 1s were also decomposed into three peaks of O^{2-} (oxides), OH^- (hydroxides or hydroxyl group), and H_2O (bound water or adsorbed water) [25]. The ratio of Ca and P ([Ca]/[P]) and the fraction of the OH^- in all oxygen atoms, $[OH^-]/([O^{2-}] + [OH^-] + [H_2O])$, are shown in Fig. 6. The [Ca]/[P] ratio increased in the order of 2.0 V for 10 ks: 1.0 V for 10 ks: 1.0 V for 1 ks : 2.0 V for 1 ks. These two data showed strong correspondence. The largest ratio in the specimen treated at 2.0 V for 10 ks was 1.75, which was almost identical to that of the hydroxyapatite nominal, 1.67. The same specimen showed the largest OH^- fraction, which was 0.75.

This calcium phosphate formation was reconfirmed by the SEM/EDS analysis. Figure 7 indicates the result of EDS analysis of the specimen treated at 1.0 V for 1 ks after immersion in Hanks' solution. The peaks from Ca and P, which are precipitated during immersion in Hanks' solution, are identified.

3.2 CP treatment

3.2.1 Current density response curves

The current density response curve during CP treatment at 1 Hz with –1.0 to 1.0 V is shown in Fig. 8. The maximum anodic current in each cycle of a potential wave decreased asymptotically when the testing time elapsed, while the minimum cathodic current exhibited a small fixed current around –5.0 A m^{-2}. In the case of the treatment at the same frequency with 0–2.0 V, a curve with the same tendency but drawn only in the anodic side (the minimum current was just on the

Table 3 Thickness and fraction of Ti^{4+} among all Ti cations (Ti^{2+}, $Ti3^{+}$, and Ti^{4+}) in the oxide film formed on the specimens with/without SP treatment

	Treatment conditions			
	Untreated	1 V–1 ks	1 V–10 ks	2 V–1 ks
Thickness of surface oxide (nm)	3.6	5.9	6.1	6.0
$[Ti^{4+}]/([Ti^{2+}] + [Ti^{3+}] + [Ti^{4+}])$	0.82	0.91	0.91	0.94

The thickness was calculated from XPS data according to Asami's inductive method [21]

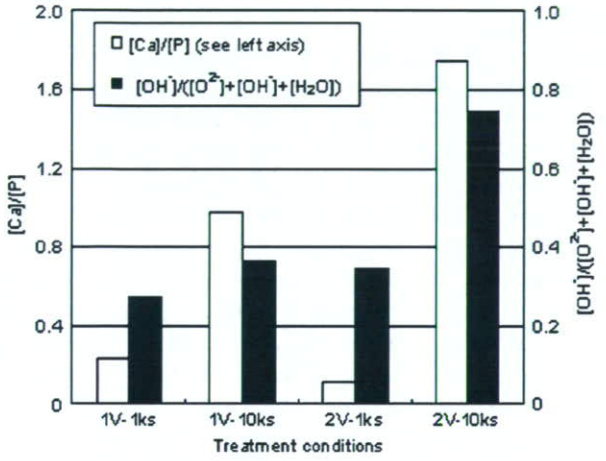

Fig. 6 Ratio of [Ca]/[P] and the fraction of the OH^- in all oxygen atoms $[OH^-]/([O^{2-}] + [OH^-] + [H_2O])$ of the surface oxide films on SP-treated specimens

abscissa) was obtained. For the CP treatments at 10 Hz with –1.0 to 1.0 V and 0–2.0 V, similar wave forms to 1 Hz with ten times faster frequency were seen.

No mark of pitting and general corrosion was observed in each specimen after these treatments.

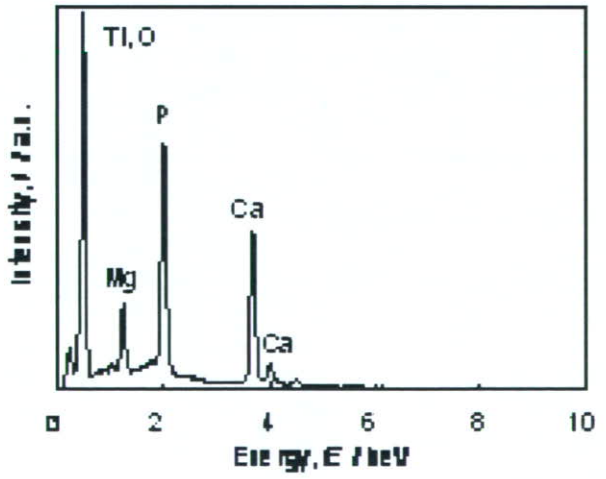

Fig. 7 SEM/EDS analysis of specimens treated at 1.0 V for 1 ks after immersion in Hanks' solution indicating peaks from Ca and P

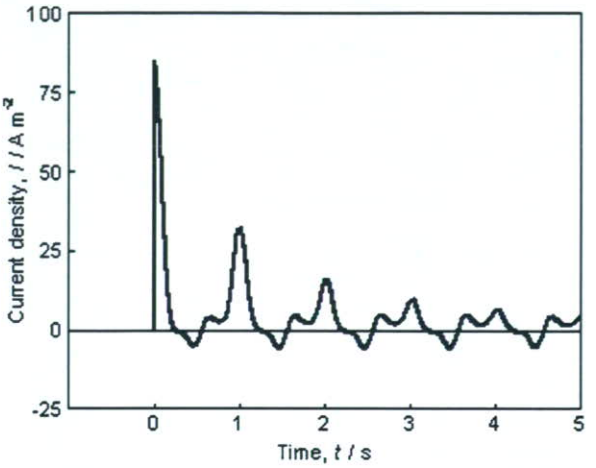

Fig. 8 Current density response curve during 1 Hz (–1_1)V CP treatment. The potential waves from were –1.0 V to 1.0 V at 1 Hz in frequency

3.2.2 XPS analysis

After the CP treatment, the surfaces of the specimens achieved a pale golden lustre, suggesting that the reaction products formed in the same way as with the SP treatment. The lustre was paler than that of SP-treated specimens at 2.0 V for 10 ks. Wide-range XPS analysis detected peaks from C, O, Ti, P, Ca, and/or N in each spectrum as well.

The compositions of the surface films are indicated in Table 4. In each specimen, O occupied around 80 mol % of the surface films, which was O^{2-}, OH^-, and H_2O. Specimens after CP treatment with 0–2.0 V exhibited higher Ti contents than those after CP treatment with –1.0 to 1.0 V.

The surface film thickness calculated from the XPS data and the fraction of Ti^{4+} in the oxide film are indicated in Table 5. Showing a certain correspondence between the thickness and Ti^{4+} fraction, the minimum of both data was seen in the specimen treated at 1 Hz with 0–2.0 V (4.9 nm in thickness and 0.88 in fraction), and the maximum, in the specimen at 10 Hz with 0–2.0 V (5.6 nm in thickness and 0.93 in fraction).

Table 4 Compositions of the surface films of the specimens after CP treatment calculated from XPS data

	Ti	O	P	Ca
1 Hz (0_2) V	21.19	77.56	1.01	0.13
1 Hz (–1_1) V	13.32	83.94	1.91	0.83
10 Hz (0_2) V	20.60	77.85	1.32	0.23
10 Hz (–1_1) V	18.15	78.84	1.41	1.60
				(mol %)

The spectra of P 2p and Ca 2p were also determined to come from PO_4^{3-}, HPO_4^{2-}, and Ca^{2+}, in the same way as for SP-treated specimens. The [Ca]/[P] ratio and the ratio of $[OH^-]/([O^{2-}] + [OH^-] + [H_2O])$ are shown in Fig. 9. For both the [Ca]/[P] ratio and the fraction of OH^-, the specimens treated with the potential wave from –1.0 V to 1.0 V were larger than those treated only with the anodic current (0–2.0 V). This suggests that the cathodic current might have an effect on calcium phosphate precipitation.

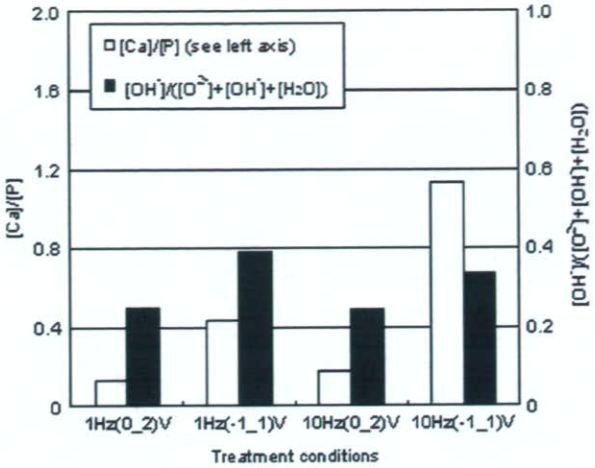

Fig. 9 Ratio of [Ca]/[P] and the fraction of the OH^- in all oxygen atoms $[OH^-]/([O^{2-}] + [OH^-] + [H_2O])$ of the surface oxide films on CP-treated specimens

3.3 Calcium phosphate formation

Figure 10 shows secondary electron images of the surface of specimens after immersion in Hanks' solution for 1.0 Ms; these images correspond to SP-treated and untreated specimens. In the EDS analysis carried out simultaneously, P, Ca, and Mg were identified in the precipitates on the surface, which suggested the formation of calcium phosphate-containing magnesium. Ban and Maruno [26] also reported that the magnesium in the calcium phosphate layer was deposited on the titanium after an electrochemical treatment using a simulated body fluid. The amount of calcium and magnesium increased proportionally to the square root of the treatment time and the cathodic potential. Comparing the SEM images, no significant difference on precipitate formation was seen between the untreated specimen and specimens treated for 1 ks. The number of calcium phosphate particles, however, obviously increased with increasing the treatment time up to 10 ks.

The results of immersion for CP-treated specimens are shown in Fig. 11. Cracks were observed in the base calcium phosphate layer formed during the CP treatment. In comparison with calcium phosphate formation during immersion, the specimens treated at –1.0 to 1.0 V showed a larger amount of precipitate.

3.4 Electrolytic treatments for titanium texture

SEM micrographs of a titanium woven texture after CP treatments at 1 Hz with –1.0 to 1.0 V followed by Hanks' solution immersion for 1.0 Ms are shown in Fig. 12. In the higher magnification on the right, calcium phosphate precipitates of around 5 μm in particle size were clearly identified with EDS. No corrosion was observed, even at higher magnification.

4 Discussion

4.1 Effects of electrolytic treatments on the surface films

The phenomenon that occurred in the electrolytic cell while the potential increased from the rest potential, E_0, to 1.0 or 2.0 V of the step potential in the SP treatment can be considered to be a charge/discharge process of the total electric charge, Q, to/from a condenser (an electric double layer) through a resistant

Table 5 Thickness and fraction of Ti^{4+} among all Ti cations in oxide film formed on the specimens after CP treatment.

	Treatment conditions			
	1 Hz(0_2) V	1 Hz (–1_1) V	10 Hz (0_2) V	1 Hz 0 (1_1) V
Thickness of surface oxide (nm)	4.9	5.3	5.6	5.1
$[Ti^{4+}]/([Ti^{2+}] + [Ti^{3+}] + [Ti^{4+}])$	0.88	0.90	0.93	0.91